Available online at www.sciencedirect.com
ScienceDirect
Journal of Nuclear Materials 359 (2006) 17–28
journal of nuclear materials
www.elsevier.com/locate/jnucmat

Modeling of constituent redistribution in U–Pu–Zr metallic fuel

Yeon Soo Kim [a,*], S.L. Hayes [b], G.L. Hofman [a], A.M. Yacout [a]

[a] Argonne National Laboratory, Nuclear Engineering, RERTR, 9700 South Cass Avenue, Argonne, IL 60439, USA
[b] Idaho National Laboratory, P.O. Box 1625, Idaho Falls, ID 83415-6188, USA

Received 28 March 2006; accepted 11 July 2006

Abstract

A computer model was developed to analyze constituent redistribution in U–Pu–Zr metallic nuclear fuels. Diffusion and thermochemical properties were parametrically determined to fit the postirradiation data from a fuel test performed in the Experimental Breeder Reactor II (EBR-II). The computer model was used to estimate redistribution profiles of fuels proposed for the conceptual designs of small modular fast reactors. The model results showed that the level of redistribution of the fuel constituents of the designs was similar to the measured data from EBR-II.

1. Introduction

Recently, the U–Pu–Zr metallic alloy has been gaining renewed attention as fuel to be used in advanced small modular fast reactors. This is a result of its proven irradiation performance [1]. Evaluation of expected fuel performance is needed for those new reactor concepts. One important issue is the redistribution of fuel constituents that alters alloy composition during irradiation, which in turn affects other fuel performance phenomena such as fuel swelling and growth.

Constituent redistribution in a metallic U–Pu–Zr alloy fuel is a commonly observed irradiation phenomenon, which was first reported in the 1960s. As shown in Fig. 1, the microstructures of the irradiated fuels exhibit three distinct concentric zones, viz., a Zr-enriched central zone, a Zr-depleted and U-enriched intermediate zone, and a slightly Zr-enriched zone on the outer periphery. The annular zone structure is also characterized by distinct differences in porosity. The presence of Pu in the alloy at levels greater than 8 wt% enhanced U and Zr migration [2]. The migration of Zr atoms is understood to be caused by the radial temperature gradients in the fuel temperature range encompassing a multi-phase regime in which each phase field has different thermochemical properties. Although there are some irregularities, in general the U profile is opposite of that of Zr. The Pu profile shows some decrease toward the fuel surface in the case of fuel element T179 used in the present analysis; however, other experimental observations [3] showed that it remained virtually unchanged.

There have been previous attempts to analyze the phenomenon of constituent redistribution for both

* Corresponding author. Tel.: +1 630 252 3173; fax: +1 630 252 5161.
E-mail address: yskim@anl.gov (Y.S. Kim).

0022-3115/$ - see front matter © 2006 Elsevier B.V. All rights reserved.
doi:10.1016/j.jnucmat.2006.07.013

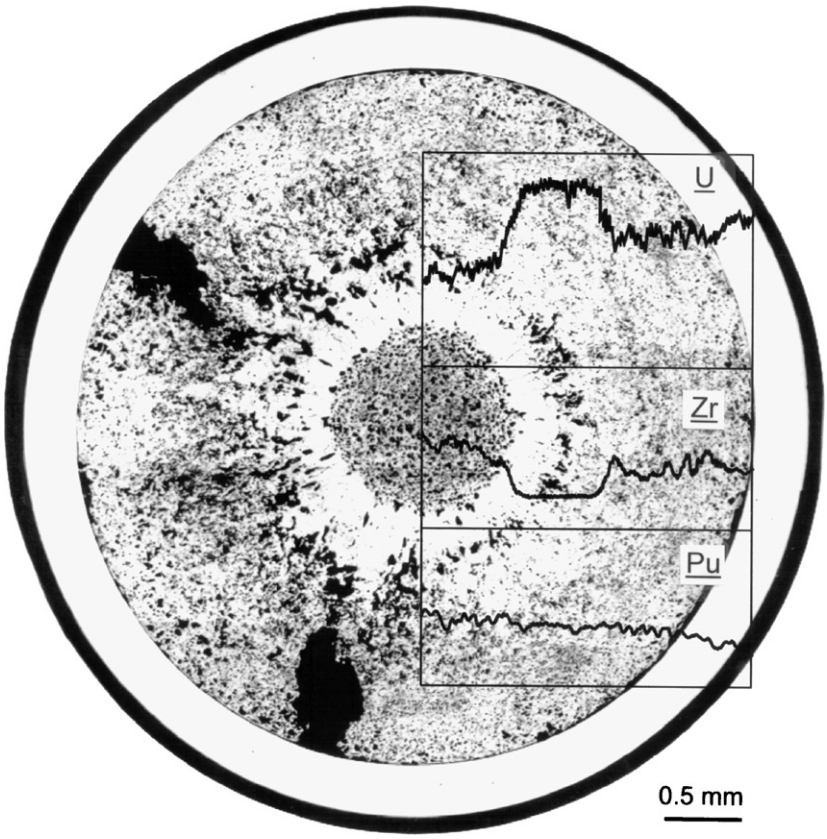

Fig. 1. Cross-sectional optical photomicrograph of the postirradiation fuel and electron probe microanalysis (EPMA) scans obtained from at an elevation of 230 mm ($z/L = 0.67$) from the fuel bottom of element T179. The Y-axis is for the uncorrected unitless concentrations of U, Pu and Zr. The scans were performed from the fuel center to the fuel surface along the X-axis.

U–Zr and U–Pu–Zr metallic alloy fuels. Ogawa et al. [4] analyzed the U–Zr system by solving the one-dimensional Fick's equation numerically. A qualitative suggestion regarding the effect of the addition of Pu in U–Zr was made. No experimental data were utilized to verify the model predictions. Hofman et al. [5] analyzed their postirradiation data to develop a computer model that predicts the redistribution in a binary U–Zr fuel. Model results were parametrically compared to measured U and Zr redistribution profiles to obtain estimates for the necessary kinetic and/or thermo-kinetic coefficients. Ishida et al. [6] extended a model by Marino [7] for the U–Zr binary system to the U–Pu–Zr ternary system. Assuming Pu was equally partitioned in U and Zr, they assessed a quasi-binary system numerically. Their model, however, predicted redistribution profiles that were shifted towards the fuel surface, which differed from measured profiles and was perhaps due to fuel temperature predictions that were too high. Kim et al. [8] assessed the kinetic and/or thermo-kinetic properties for irradiated U–Pu–Zr fuel based on redistribution profiles measured at the end of fuel life. By utilizing the method proposed by Sohn et al. [9], the constituent interdiffusion fluxes of U, Pu and Zr at the end of fuel life were calculated without the need or knowledge of ternary interdiffusion coefficients ($\tilde{D}_{ij}^{k}$'s) and heats of transport ($\tilde{Q}_i$). The calculated interdiffusion fluxes were then employed to obtain effective interdiffusion coefficients and heats of transport.

As a prediction method of the kinetics of constituent redistribution, we developed a computer model [10] applicable to fuel constituent redistribution in ternary U–Pu–Zr alloy fuels by extending the model used for U–Zr binary alloy fuels in Ref. [5]. The new computer model calculates Zr redistribution by solving diffusion equations using a simplified pseudo-binary phase diagram, treating Pu to be immobile, and by enhancing diffusion and thermo-

chemical properties from the U–Zr binary case. Because there was no measured data available, a parametric study was performed to obtain the effective diffusion and thermochemical properties by assessing agreement with measured data.

In addition, the model was used to assess redistribution of constituents for two of the proposed fuel designs to be used in future advanced fast reactors, that is, 4S and SMFR fuel designs. The results showed that constituent redistribution of the fuel for these fuel designs was not severe given the proposed range of operating conditions.

2. Phase diagram

Because the thermochemical driving force for constituent migration is affected by the various phases present in the fuel at operating temperatures, establishing an accurate estimation of the phase diagram for the ternary U–Pu–Zr alloy fuels is critical in the development of the computer model. Based on the available ternary phase diagrams [11,12] for temperatures of interest, and by fixing the Pu concentration at 16 at.% (19 wt%), a pseudo-binary (U–Pu)–Zr phase diagram was formulated. Fig. 2 shows the partial pseudo-binary phase diagram developed in this manner.

The phase diagram shown in Fig. 2, however, was unnecessarily complex for implementation in the computer model. First, the U + Pu rich side is composed of small phase fields. Second, the phase boundaries between the large-phase fields of the $\zeta + \gamma$, $\zeta + \delta + \gamma$, $\zeta + \delta$, and $\alpha + \zeta + \delta$ are slanted against the abscissa, which makes programming difficult. A simplified version was developed. There are two main features in the simplification. First, the phase fields on the U + Pu rich side was simplified by using the $(\alpha + \zeta)$ and $(\beta + \zeta)$ phases for this region. The $(\alpha + \zeta)$ and $(\beta + \zeta)$ are pseudo-single phases that possess characteristics of the mixture of α and ζ, and β and ζ, respectively. Second, the slanted phase boundaries mentioned above were made parallel to the abscissa. The result is the phase diagram shown in Fig. 3. Although there are differences in detail, Fig. 3 turned out to be similar to that reported by Ishida [6]. This pseudo-binary phase diagram may appear overly simplified; however, it was effective in overcoming the unnecessary complexity posed by dealing with ternary phase diagrams in programming.

In Fig. 3, the radial Zr concentration profile of T179 at 1.9 at.% burnup (the broken line) and at BOL (dotted line) are also superimposed. The EOL zone boundaries match well with the phase boundaries between the γ and the $(\beta + \zeta) + \gamma$ and between the $(\beta + \zeta) + \gamma$ and the $(\alpha + \zeta) + \delta$. Basically, this is because the corresponding temperature distribution [8] was obtained by fitting to the redistribution profile, which will be discussed in detail in the next section. The $\gamma 1$ phase is a U-rich modification and the $\gamma 2$ is a Zr-rich modification of the γ phase.

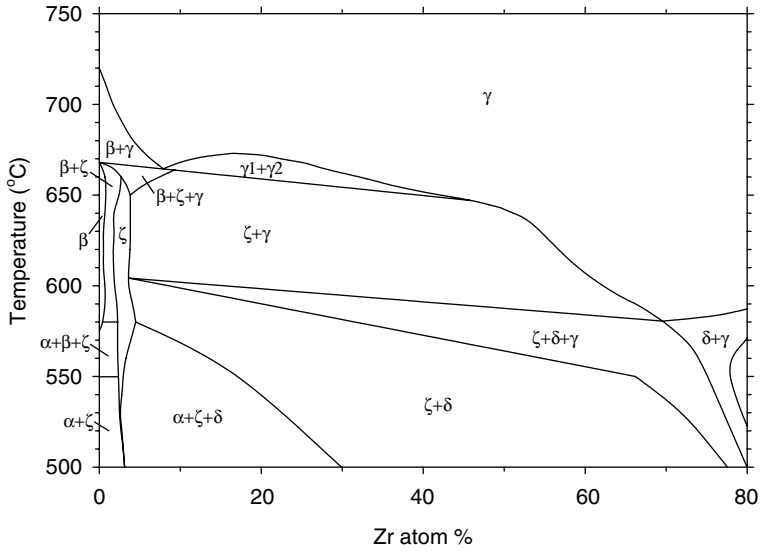

Fig. 2. Pseudo-binary (U–Pu)–Zr phase diagram of the fixed Pu content at 19 wt%.

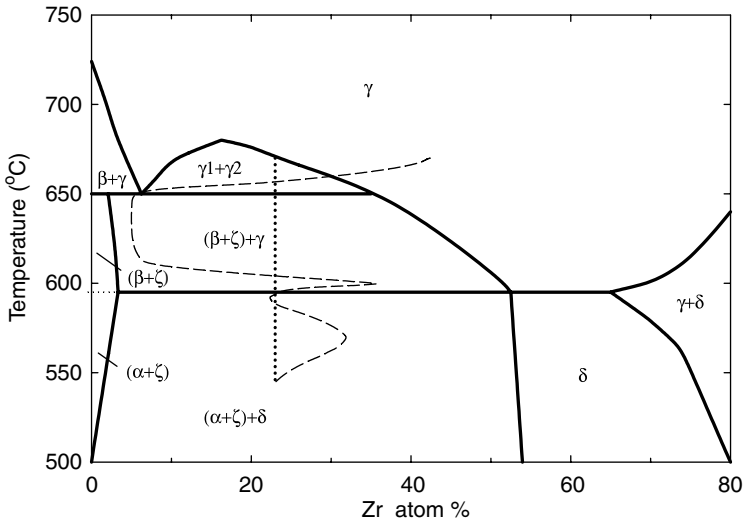

Fig. 3. Simple pseudo-binary phase diagram of (U–Pu)–Zr of the Pu content of 19 wt% used in the computer program. The Zr concentration profiles of T179 at the beginning of life (dotted line) and at the end of life (broken line) are also superimposed.

When applied to a fuel with different Pu content, the phase diagram must be modified accordingly. In particular, the temperatures for the phase boundaries between the $\gamma 1 + \gamma 2$ and the $(\beta + \zeta) + \gamma$, and between the $(\beta + \zeta) + \gamma$ and the $(\alpha + \zeta) + \delta$, must be changed. For example, if the Pu content decreases from the typical content of 19 wt% to 15 wt%, the phase boundary temperatures will slightly increase (~20 °C). For most cases, however, the Pu content is close to 19 wt% so that the phase diagrams in Fig. 2 and in turn Fig. 3 can be applied without any modifications.

3. T179 temperature distribution

The fuel temperature distribution used in the parametric study is shown in Fig. 4. This temperature distribution is a combination of prediction and experimental observation utilized by Kim et al. for their analyses [8]. However, fuel tempera-

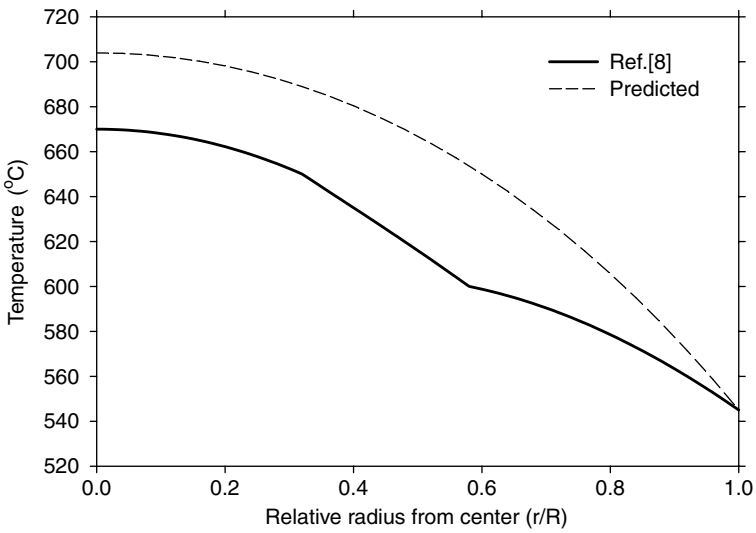

Fig. 4. Calculated temperature distributions of T179 fuel at the axial location of 230 mm from the bottom of fuel at BOL. The dashed line represents prediction by the computer program, and the solid line is taken from Ref. [8].

tures are normally calculated with a computer program using the scheme in Ref. [5], where the fuel power at the particular radial ring depends on the actinide concentration in the ring, and the fuel conductivity changes due to the evolution of porosity. For most calculations, the fuel conductivity continuously decreases to ~50% of the BOL value until approximately 0.75 at.% burnup, and then increases linearly up to ~70% at 1.5 at.% burnup as sodium infiltrates into the pores and cracks that develop in the rapidly swelling fuel. After 1.5 at.% burnup, the fuel conductivity remains essentially constant at ~70% of the BOL value.

4. Irradiation experiment

The fuel pin selected for the present study was from an experimental sub-assembly irradiated during the Integral Fast Reactor (IFR) fuel development program [8]. The fuel pin was designated as T179 from experiment X419 and was extensively characterized during postirradiation examinations following reactor discharge. Fabrication and operational parameters are given in Table 1. The fuel element was irradiated in the Experimental Breeder Reactor II (EBR-II) for two consecutive cycles, 49 days in Run-133 and 43 days in Run-134 achieving the final peak burnup of 1.9 at.%.

5. Model development

Only radial Zr migration is considered as axial temperature gradients are relatively small and axial Zr redistribution has not been experimentally observed. The one-dimensional continuity equation for Zr in cylindrical coordinates may be expressed as

$$\frac{\partial C_{Zr}}{\partial t} = -\frac{1}{r}\frac{\partial (r\tilde{J}_{Zr})}{\partial r} + s, \tag{1}$$

where C_{Zr} is the Zr concentration, $\tilde{J}_{Zr}$ the interdiffusion flux and s the Zr production rate by fission. The Zr yield per U atom fission is 0.29 and that for Pu atom fission is 0.20.

Within a single-phase field, as was given in Ref. [5], the Zr interdiffusion flux is given by

$$\tilde{J}_{Zr} = -\tilde{D}^{eff}_{Zr}\left(\frac{\partial C_{Zr}}{\partial r} + \frac{\tilde{Q}_{Zr}C_{Zr}}{RT^2}\frac{\partial T}{\partial r}\right), \tag{2}$$

where $\tilde{D}^{eff}_{Zr}$ is the effective interdiffusion coefficient of Zr in U–Pu–Zr, $\tilde{Q}_{Zr}$ the heat of transport of Zr in U–Pu–Zr, R the gas constant, and T the temperature. Eq. (2), a pseudo-binary equation for the Zr flux, is convenient for use in simplifying the model. This is justified as long as the proper diffusion properties, $\tilde{D}^{eff}_{Zr}$ and $\tilde{Q}_{Zr}$, are provided. Referring to the phase diagram, the single phase occurs only at high temperatures above ~650 °C, and the corresponding phase is the γ-phase. Therefore, Eq. (2) applies solely to the γ-phase.

Within a dual phase field (strictly speaking, these are pseudo-dual phase fields, such as $(\beta+\zeta)+\gamma$ and $(\alpha+\zeta)+\delta$), the driving force for diffusion is affected by the solubility of Zr in the precipitation phases, $(\beta+\zeta)$ and $(\alpha+\zeta)$ for the present case. This changes the Zr concentration in the continuous phase, given by the γ and δ for the present case. The terminal solubility of Zr in the $(\beta+\zeta)$ and $(\alpha+\zeta)$ is described by

$$C_{Zr} = C^0_{Zr}\exp\left(-\frac{\overline{\Delta H}_s}{RT}\right), \tag{3}$$

where $\overline{\Delta H}_s$ are the partial molar enthalpies of solution of Zr in the fuel for each phase field. Therefore, the corresponding flux equation in a dual phase field is obtained by substituting Eq. (3) into Eq. (2) as follows:

$$\tilde{J}_{Zr} = -\tilde{D}^{eff}_{Zr}C_{Zr}\frac{\overline{\Delta H}_s + \tilde{Q}_{Zr}}{RT^2}\frac{\partial T}{\partial r}. \tag{4}$$

From Eqs. (2) and (4), it is noticeable that the Zr flux in a single phase is caused by the concentration gradient and the temperature gradient. In a dual phase field, however, only the temperature gradient

Table 1
Fuel fabrication and operation data for the fuel element T179 [8]

Fuel alloy nominal composition (wt%)	U–19Pu–10Zr
Fuel alloy nominal composition (at.%)	U–16Pu–22Zr
^{235}U concentration in U (%)	56.99
Fuel slug length (mm)	342.9
Fuel slug radius (mm)	2.16
Fuel slug density (g/cm^3)	15.8
Fuel smeared density (%)	72.3
Fuel-cladding gap material	Liquid Na
Sodium level above fuel (mm)	6.35
Cladding thickness (mm)	0.381
Fuel-cladding gap width (mm)	0.762
Linear heat rate (W/cm)	420
Subassembly coolant temperatures (°C)	Inlet: 371 Outlet: 486
Subassembly coolant flow rate (liter/s)	7
Irradiation burnup (at.% total HM)	1.9

has a direct effect, whereas the concentration gradient is an indirect effect. Because the temperature gradient is always negative, the sign of $(\overline{\Delta H}_s + \tilde{Q}_{Zr})$ determines the direction of the Zr flux. If it is positive, the Zr flux also becomes positive, and the direction of Zr migration in this case is toward the fuel surface; alternatively, a negative Zr flux would indicate Zr migration toward the fuel center.

Casting Eq. (1) in finite-difference form gives

$$C_{Zr}^{i,j} = C_{Zr}^{i,j-1} + 2\Delta t \frac{r^{i-1}\tilde{J}_{Zr}^{i-1,j} - r^{i+1}\tilde{J}_{Zr}^{i+1,j}}{(r^{i+1})^2 - (r^{i-1})^2} + \Delta t s^j, \qquad (5)$$

where Δt is the time-step size, i the ith radial ring and j the jth time-step. Eq. (5) is solved using the flux equations given by Eqs. (2) and (4). The maximum time-step size is restricted by the stability criterion

$$\Delta t < \frac{(\Delta r)^2}{2\tilde{D}_{Zr}^{eff}}$$

to generate a valid calculation, where Δr is the radial spatial-step size and $\tilde{D}_{Zr}^{eff}$ is the effective interdiffusion coefficient of Zr. To satisfy this criterion, the computer program divides the time-step further and iterates the whole calculation process internally for the sub-time-steps.

6. Model parameters

6.1. Effective interdiffusion coefficient

The interdiffusion coefficient $\tilde{D}_{Zr}^{eff}$ for U–Pu–Zr is not available. Therefore, it was estimated parametrically. The interdiffusion coefficients for U–Zr binary alloy are available in Ref. [5] and are given in Table 2. Although these data are not directly applicable for the ternary case, they can be used as base information in the parametric study.

The influence of Pu addition and irradiation on the Zr migration kinetics is handled by enhancement factors, which are multiplied by the U–Zr out-of pile data. The existence of Pu in a ternary fuel greatly increases the interdiffusion coefficient. There are reports that the interdiffusion coefficient of Zr in the γ-phase of U–Pu–Zr fuel could increase an order of magnitude when the Pu content is at least 8 wt% and increases with the Pu content [1,2]. Using this information, the enhancement factors for Zr interdiffusion coefficients for relevant phases were sought at the similar magnitude by fitting with T179 data. The best combination of the enhancement factors for each phase to simulate T179 profiles was found as follows:

γ phase: 13
β + ζ phase: 20
α + ζ phase: 15
δ phase: 15

Additionally, the effective interdiffusion coefficient for the contiguous phase with more than 50 vol.% in a two phase mixture was enhanced by a factor of 10 for $595 \leqslant T \leqslant 650$ °C and by a factor of 6 for $T \leqslant 595$ °C in order to take into account the effect of the ζ phase. By this enhancement, prediction gave a good fit to the T179 data.

In order to compare the effective interdiffusion coefficients obtained in the present study with values from an analytical analysis of the measured composition profiles using the so-called zero flux plane method [8], the effective interdiffusion coefficients as a function of radial position were averaged for each radial zone. A comparison is provided in Table 3. The zone-average interdiffusion coefficients obtained in the present study are close to those of Ref. [8], but they are generally larger than those from Ref. [8], particularly in the outer zone. The difference in the outer zone is attributed to the different concentration profile used in Ref. [8]. For the purpose of the analytical analysis in Ref. [8], the measured concentration profile originally with abrupt changes and choppiness as in Fig. 1 was smoothed. In this respect, the most affected zone is the outer zone. In the concentration profile in Ref. [8], the concentration has a maximum at $\sim 0.85r/R$ in the outer zone while in the present case it generally decreases

Table 2
Out-of-pile interdiffusion coefficients in $\tilde{D} = \tilde{D}_0 \exp(-Q/RT)$ for U–Zr alloy [5]

	γ	β + ζ	α + ζ	δ
$\tilde{D}_0$ (m²/s)	$\exp(-6.15 + 18.5x_{Zr} - 21.0(x_{Zr})^2)$	5.7×10^{-7}	2.0×10^{-7}	2.0×10^{-7}
Q (kJ/mol)	$128 - 107x_{Zr} + 174(x_{Zr})^2$	180	170	150

Where x_{Zr} is the Zr mole fraction.

Table 3
Zone average $\tilde{D}_{Zr}^{eff}$ at the EOL of T179

Redistribution zone	Zone average $\tilde{D}_{Zr}^{eff}$ (10^{-14} m^2/s)	
	Ref. [8]	Present study
Center	2.8	3.4
Intermediate	0.87	1.1
Outer	0.14	0.74

toward the fuel surface at $\sim 0.7 < r/R$. Considering the unstable nature in this zone because of swelling, pore connection, and sodium infiltration, it is uncertain at this time which case is real. More experimental data can only resolve this uncertainty.

6.2. Enthalpy of solution

The enthalpies of solution of Zr in the dual phases $(\beta + \zeta) + \gamma$ and $(\alpha + \zeta) + \gamma$ of U–Pu–Zr were estimated by using the Kohler equation for the Gibbs energy of the ternary solution phases [13] and data for the excess Gibbs free energy of Zr solution in the γ-phase of the U–Pu–Zr alloy available from Ref. [14]:

$$\begin{aligned} G_{Zr}^{E} &= RT\ln(\gamma_{Zr}) \\ &= x_U^2(43764.5 - 22.0T - 44174.7x_{Zr} + 38635.1x_{Zr}^2) \\ &\quad + x_{Pu}^2(6574.7) + x_U x_{Pu}(15884.0), \end{aligned} \tag{6}$$

where G_{Zr}^{E} is the excess Gibbs free energy in J/mol, γ_{Zr} the activity coefficient of Zr, x the mole fraction and T the temperature in K.

Using the γ_{Zr} from Eq. (6), the enthalpy of solution can be calculated by the relation

$$\overline{\Delta H}_s = -RT^2 \frac{\partial \ln \gamma_{Zr}}{\partial T}. \tag{7}$$

Substituting Eq. (6) into Eq. (7) gives

$$\overline{\Delta H}_s = G_{Zr}^{E} - T\frac{\partial G_{Zr}^{E}}{\partial T}. \tag{8}$$

The first term in the right hand side of Eq. (6) is the excess Gibbs free energy of U–Zr [14]. If the Pu content is zero, Eq. (6) goes to that of U–Zr, giving weight to its validity. Furthermore, although there are extra terms involving the Pu content, G_{Zr}^{E} for U–10Zr and U–19Pu–10Zr are close to each other. This in turn produces a similar enthalpy of solution to that of U–Zr.

As the γ phase is the continuous phase at high temperatures for the $(\beta + \zeta) + \gamma$ phase, so is the δ phase at low temperatures (<595 °C for U–19Pu–10Zr) for the $(\alpha + \zeta) + \delta$. Therefore, Eqs. (6) and (7) were also used for the δ phase. Because the temperature is low, however, the mobilities are low and the magnitude of the model parameters for this phase do not significantly influence the results of the calculations.

6.3. Effective heat of transport

The heats of transport for each phase field were obtained parametrically to reproduce the shape and extent of the measured redistribution profile of T179 [8], and the results are as follows:

γ phase: −200 kJ/mol,
$\beta + \zeta$ phase: 450 kJ/mol,
$\alpha + \zeta$ phase: 200 kJ/mol,
δ phase: 160 kJ/mol.

The heat of transport in the γ phase is larger than the suggested range between −50 and −100 kJ/mol for U–Zr [5]. The negative heat of transport in the γ phase generates the driving force for Zr to migrate toward fuel center, against the concentration gradient even after Zr accumulation in the center region has considerably progressed. The positive heats of transport for the $\beta + \zeta$, $\alpha + \zeta$ and δ phases, however, make Zr migrate toward the fuel surface if they are larger than the magnitude of the enthalpy of solution. The heats of transport obtained here are phenomenological effective values that we have to use to fit the measured redistribution profile.

Similar to the interdiffusion coefficient, the increase in the heat of transport also increased the magnitude of redistribution. However, the heat of transport together with the enthalpy of solution, i.e., the sign of $\overline{\Delta H}_s + \tilde{Q}_{Zr}$, determines the direction of Zr migration, and in turn the shape of the redistribution profile.

7. Model predictions and discussion

The following sections describe the verification of the model predictions when compared to the measured data for pin T179. In addition, the redistribution profiles in fuel pins to be used in new fast reactor design concepts (4S and SMFR) are predicted using the model.

7.1. T179

The measured X-ray intensity profile of Zr redistribution, shown in Fig. 1, was corrected on the basis of mass conservation throughout the fuel

cross-section. The values for every $0.02r/R$ were determined and plotted in Fig. 5. In the intermediate zone, the Zr concentration is ~5 at.%, which is close to the phase boundary between the $(\beta+\zeta)$ and $(\beta+\zeta)+\gamma$. This minimum Zr concentration was included in the computer model.

Predictions by the computer model were made using the parameters determined in the previous section together with the basic data and the temperature distribution (the solid line in Fig. 4). The pin power decreased as burnup increased. The calculation result is compared with the measurement in Fig. 5. Only the Zr redistribution profile is given. Since the Pu concentration is fixed at 0.16 atom fraction, the U concentration profile can be obtained by subtracting the Zr concentration from 0.84. In general, the predictions are in good agreement with the measured data except for the shift ($\sim 0.05r/R$) of the zone boundaries toward the fuel surface. The positions of zone boundaries are indicators of fuel temperature distribution because the positions of the zone boundaries are determined as a result of phases the fuel experiences during irradiation. The zone boundaries move toward the fuel surface as the fuel temperature increases, and vice versa. Therefore, the shift of the positions of the zone boundaries from the measured data more toward the fuel surface than the prediction indicates that the fuel temperatures during irradiation were likely somewhat lower than those used for the calculation. When a temperature distribution (for example, the broken line in Fig. 4 for BOL) that was simultaneously updated with fissile element redistribution in the computer model was used, the discrepancy between the prediction and the measurement became worse, with a more shifting of the zone boundaries toward the fuel surface (i.e., $\sim 0.2r/R$) than the fixed temperature case ($\sim 0.05r/R$). All of these factors suggest that using an accurate fuel temperature distribution is very important for achieving a good redistribution prediction. As seen in Fig. 1, the fuel cross-section shows two large cracks reaching to the periphery of the intermediate zone. In addition, numerous smaller cracks were apparently interconnected at the end of the large pore, extending the effective pore interconnection to the middle of the intermediate zone, and suggesting a possibility of an even higher order of pore interconnection. During the gap closure, liquid sodium is relocated from the gap between the fuel and cladding into these cracks and pore structure. As a result, the effective fuel conductivity can increase significantly. Therefore, the actual fuel temperature and its gradient were likely lower than the calculated values used in this analysis, which neglected these local effects.

There is a minor increase in the Zr concentration toward the fuel surface, although it is choppy in nature. The calculated results follow the general trend of the measured data, with the peaking near the boundary between the intermediate zone and the outer zone, demonstrating the predictive capability

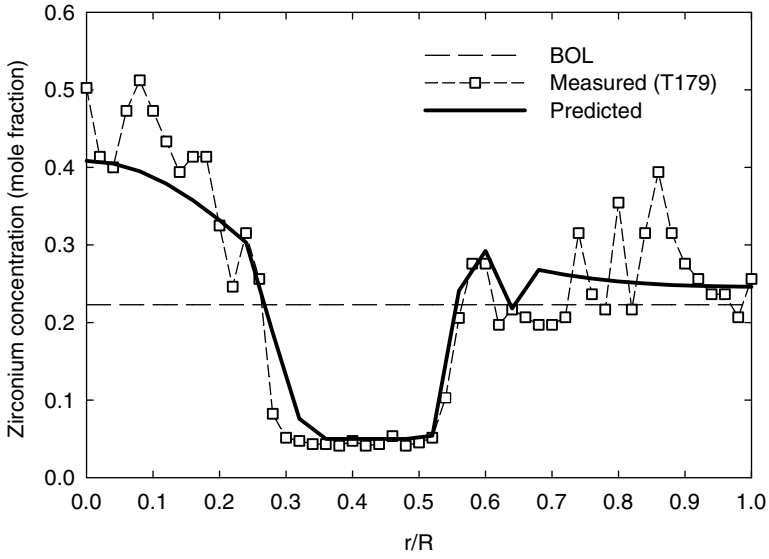

Fig. 5. Comparison of Zr redistribution profiles of T179 by the prediction and by the measurement.

of the computer model. The prediction result also exemplifies the reasonableness of the simplified pseudo-binary phase diagram used by the model.

7.2. 4S

One of the fuel designs for the conceptual 4S (Super Safe, Small and Simple) reactor [15] uses U–Pu–Zr alloy. As part of the preliminary design evaluation, fuel constituent redistribution was predicted. The design matrix used for the prediction is given in Table 4.

In Fig. 6, the predicted results are shown for three cases of fuel surface temperature for Design 1. The fuel power and surface temperature for each case were set constant throughout the fuel life. Constituent redistribution was completed at 3.7 at.% burnup for the 535 °C case, 7.5 at.% burnup for the 555 °C case and 3.2 at.% burnup for the 605 °C case of Design 1. The completion of redistribution in the middle of life represents a steady state, the result of balance between the Zr flux caused by the temperature and its gradient and that generated by the concentration gradient.

The highest fuel-surface-temperature case (605 °C) shows that the Zr atoms generally migrate toward the fuel center region with a minor migration component toward the fuel surface region because the fuel temperature is above 595 °C. The boundary temperature between the $(\beta + \zeta) + \gamma$ and the $(\alpha + \zeta) + \delta$ phases is 595 °C. For this case, only a weak driving force for Zr migration toward the fuel surface is created at the fuel periphery.

Similar predictions were made for Design 2. The results are given in Fig. 7. The differences between Design 1 and Design 2 are fuel radius and power; Design 2 has a larger fuel radius and higher power than Design 1, and results in a higher fuel temperature. This in turn drives in more substantial redistribution in Design 2. The completion in redistribution was also predicted at 6.5 at.% burnup for the 535 °C case and 3.0 at.% burnup for the 555 °C case. However, it is still in progress at the end of the fuel life for the 605 °C case. If compared, Figs. 6 and 7 are very similar in the shape of redistribution profiles. In Fig. 7, the redistribution profiles are slightly shifted toward the fuel surface, and they have smaller widths for the Zr-depleted zones than those of

Table 4
Proposed 4S fuel design parameters [15]

	Design 1		Design 2	
Fuel type (wt%)	U–20Pu–10Zr		U–20Pu–10Zr	
Fuel length, m	2.50		2.50	
Fuel density, g/cm^3	15.80		15.80	
Slug radius, mm	4.83		5.635	
Clad inner diameter, mm	10.80		12.60	
Linear power (at 6th node), W/cm	197		345	
Peak inner clad temperature (at top of fuel), °C	600		600	
Fuel surface temperatures, °C	Case 1	535	Case 1	535
	Case 2	555	Case 2	555
	Case 3	605	Case 3	605
Average burnup, GWd/t (at.%)	81 (8.6)		61 (6.5)	
Estimated peak fuel temperatures (at axial 6th node), °C	Case 1	671	Case 1	745
	Case 2	684	Case 2	755
	Case 3	722	Case 3	790
Axial node (from bottom of fuel)	Power shape factors			
1	0.588		0.588	
2	0.979		0.979	
3	1.229		1.229	
4	1.333		1.333	
5	1.343		1.343	
6	**1.233**		**1.233**	
7	1.071		1.071	
8	0.813		0.813	
9	0.463		0.463	

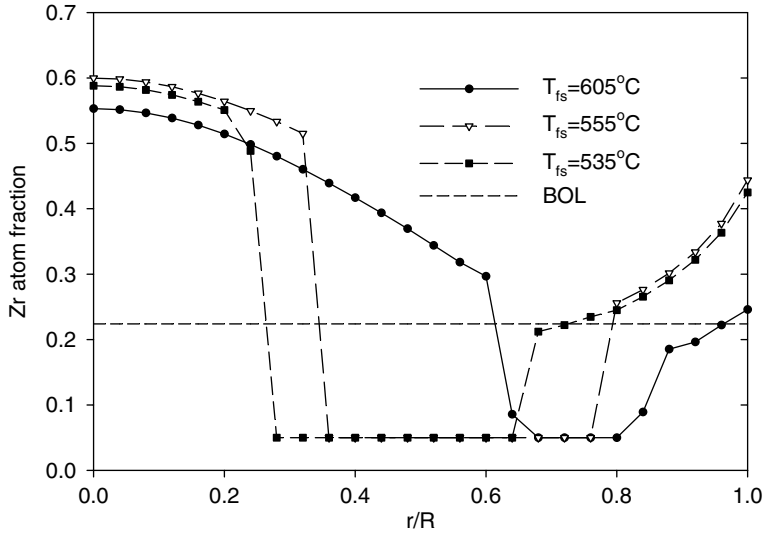

Fig. 6. Zr redistribution profiles of 4 S fuel for three fuel surface temperature cases (Design 1). The fuel power and surface temperature (T_{fs}) were unchanged throughout the fuel life.

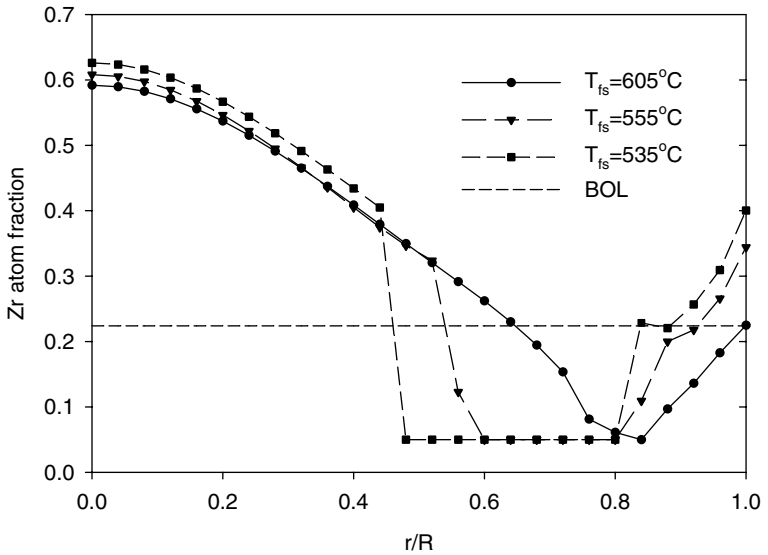

Fig. 7. Zr redistribution profiles of 4S fuel for three fuel surface temperature cases (Design 2). The fuel power and surface temperature (T_{fs}) were unchanged throughout the fuel life.

Design 1 since Design 2 has generally higher fuel temperatures.

7.3. SMFR

A reduced-Pu content is being considered in the U–Pu–Zr metallic fuel for the conceptual SMFR (Small Modular Fast Reactor) [16]. The Pu content is slightly less than 15 wt%. The proposed design parameters are given in Table 5. Because the Pu content in the alloy was significantly different from the one used to develop the phase diagram in Figs. 2 and 3, a new phase diagram was needed. The same procedure used to develop the phase diagrams in Figs. 2 and 3 was followed. As a result, the new phase diagram has the same overall shape but it is shifted in the positive direction on the temperature axis.

Table 5
SMFR fuel design parameters [16]

	IC03	MC02
Fuel type (wt%)	U–14.89Pu–10Zr	U–14.89Pu–10Zr
Fuel length (L), cm	100	100
Fuel density, g/cm^3	15.67	15.67
Fuel slug radius, cm	0.6712	0.6712
Radial fuel-cladding gap, cm	0.1038	0.1038
Linear power (at $z/L = 0.67$), W/cm	210.3 (BOL)	292.3 (BOL)
	287.6 (EOL)	269.7 (EOL)
Fuel surface temperatures, °C	472.6 (BOL)	515.9 (BOL)
	533.4 (EOL)	506.7 (EOL)
Burnup, GWd/tHM	105 (Average)	122 (Average)
	120 (at $z/L = 0.67$)	140 (at $z/L = 0.67$)
Predicted peak fuel temperatures (at $z/L = 0.67$), °C	668 (EOL)	704 (5 GWd/tHM)
Axial location from bottom of fuel	Power shape factors	
0	0.68	0.68
0.08	0.85	0.85
0.17	1.01	1.01
0.25	1.11	1.11
0.33	1.20	1.20
0.42	1.24	1.24
0.50	1.25	1.25
0.58	1.21	1.21
0.67	**1.14**	**1.14**
0.75	1.02	1.02
0.83	0.88	0.88
0.92	0.69	0.69
1	0.47	0.47

Two sample fuel pins, IC02 and MC02, were selected and analyzed. The fuel temperature and power for IC02 were gradually increased to the end of the life whereas those of MC02 were decreased. Generally, SMFR fuel has lower fuel temperatures than T179. Fig. 8 shows the calculation results.

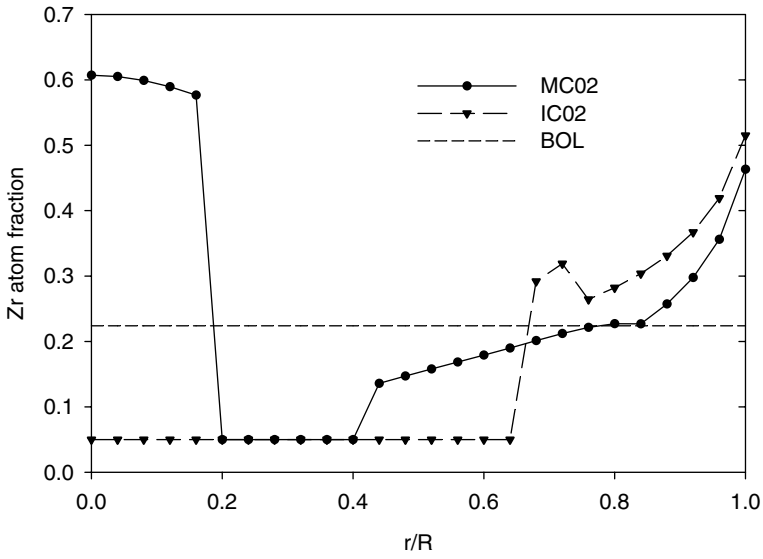

Fig. 8. Zr redistribution profiles of SMFR fuel elements (IC02 and MC02).

IC02 shows a gross Zr-depleted zone for a large portion of the fuel cross-section, indicating no γ-phase formation at the fuel center region. This happens due to the dominance of the outward flux compared to the inward one. Because the fuel temperature is generally low, the fuel resides in the lower temperature phases, $(\beta+\zeta)+\gamma$ and $(\alpha+\zeta)+\delta$. Furthermore, as discussed earlier, $\overline{\Delta H_s}+\tilde{Q}_{Zr}$ for the $(\alpha+\zeta)+\delta$ is always positive and that for the $(\beta+\zeta)+\gamma$ also becomes positive because the γ-phase fraction, which has a negative heat of transport, is smaller than the $\beta+\zeta$ as the Zr concentration decreases.

Both pins have high burnup levels. There was considerable Zr production due to the fission yield for high burnup. As a result, the Zr concentration profile was generally shifted upward and the average Zr concentration along the fuel radius is greater than the BOL value. We considered the destruction rate and production rate of Pu approximately the same.

In spite of the high burnup levels, the level of redistribution for both pins is similar to that of T179. This suggests that fuel temperature and its gradient might have more important effect than burnup or irradiation time on constituent redistribution.

8. Conclusions

A computer model was developed to calculate the redistribution of constituents in U–Pu–Zr metallic fuel under irradiation. The effective interdiffusion coefficients were parametrically determined by enhancing ~15 times the out-of-pile literature data to obtain a fit to the measured data.

The extent of redistribution, including the Zr-depletion in the intermediate fuel zone, could be reproduced when a heat of transport for the γ-phase was approximately −200 kJ/mol and that for the $\beta+\zeta$ phase was +450 kJ/mol. For the lower temperature phases, the effect of heat of transport was insignificant.

Prediction results showed that proposed fuel designs for the 4 S and SMFR reactor concepts generate similar constituent redistribution to T179 fuel, implying that the fuel temperature and its gradient are more important than burnup for redistribution kinetics, and particularly the shape of the redistribution profile is determined by the temperature distribution in the fuel.

Acknowledgements

This work has been created by the University of Chicago as Operator of Argonne National Laboratory under Contract No. W-31-109-ENG-38 with the US Department of Energy.

References

[1] G.L. Hofman, L.C. Walters, in: R.W. Cahn, P. Haasen, E.J. Kramer (Eds.), Materials Science and Technology, vol. 10A, VCH, New York, 1993.
[2] D.L. Porter, C.E. Lahm, R.G. Pahl, Metall. Trans. A 21A (1990) 1871.
[3] M.K. Meyer, S.L. Hayes, D.C. Crawford, R.G. Pahl, H. Tsai, in: Proceedings of ANS Conference on Accelerator Applications in the New Millennium, Reno, NV, November 11–15, 2001.
[4] T. Ogawa, T. Iwai, J. Less-Common Met. 175 (1991) 59.
[5] G.L. Hofman, S.L. Hayes, M.C. Petri, J. Nucl. Mater. 227 (1996) 277.
[6] M. Ishida, T. Ogata, M. Kinoshita, Nucl. Technol. 104 (1993) 37.
[7] G.P. Marino, Nucl. Sci. Eng. 49 (1972) 93.
[8] Yeon Soo Kim, G.L. Hofman, S.L. Hayes, Y.H. Sohn, J. Nucl. Mater. 327 (2004) 27.
[9] Y.H. Sohn, M.A. Dayananda, G.L. Hofman, R.V. Strain, S.L. Hayes, J. Nucl. Mater. 279 (2000) 317.
[10] Yeon Soo Kim, S.L. Hayes, G.L. Hofman, A.M. Yacout, Trans. Am. Nucl. Soc. 93 (2005) 755.
[11] D.R. O'Boyle, A.E. Dwight, The uranium–plutonium–zirconium alloy system, in: Proceedings of the 4th International Conference on Plutonium and Other Actinides, Santa Fe, NM, Met. Soc., New York, 1970, p. 720.
[12] M. Kurata, CALPHAD 23 (1999) 305.
[13] F. Kohler, Monats. Chem. 91 (1960) 738.
[14] L. Leibowitz, R.A. Blomquist, A.D. Pelton, J. Nucl. Mater. 167 (1989) 76.
[15] T. Yokoyama, N. Ueda, An optimization study on the reflector-controlled long life LMR core aiming at a negative sodium void reactivity, in: 11th International Conference on Nuclear Engineering, Tokyo, Japan, April 20–23, 2003.
[16] W.S. Yang, Argonne National Laboratory, personal communications, 2005.